# POLITECNICO DI TORINO
## Repository ISTITUZIONALE

Self-assembled poly-catenanes from supramolecular toroidal building blocks

(Article begins on next page)

04 May 2024

# Self-assembled poly-catenanes from supramolecular toroidal building blocks

Sougata Datta[1], Yasuki Kato[2], Seiya Higashiharaguchi[2], Keisuke Aratsu[2], Atsushi Isobe[2], Takuho Saito[2], Deepak D. Prabhu[1], Yuichi Kitamoto[3], Martin J. Hollamby[4], Andrew J. Smith[5], Robert Dagleish[6], Najet Mahmoudi[6], Luca Pesce[7], Claudio Perego[7], Giovanni M. Pavan[7,8] & Shiki Yagai[1,2,3]*

[1]Department of Applied Chemistry and Biotechnology, Graduate School of Engineering, Chiba University, 1-33 Yayoi-cho, Inage-ku, Chiba 263-8522, Japan.

[2]Division of Advanced Science and Engineering, Graduate School of Science and Engineering, Chiba University, 1-33 Yayoi-cho, Inage-ku, Chiba 263-8522, Japan.

[3]Institute for Global Prominent Research (IGPR), Chiba University, 1-33 Yayoi-cho, Inage-ku, Chiba 263-8522, Japan.

[4]School of Chemical and Physical Sciences, Keele University, Keele, Staffordshire ST55BG, UK.

[5]Diamond Light Source Ltd., Diamond House, Harwell Science and Innovation Campus, Didcot, Oxon OX11 0DE, UK.

[6]ISIS Pulsed Neutron and Muon Source, Rutherford Appleton Laboratory, Chilton, Oxon, OX11 0QX, UK.

[7]Department of Innovative Technologies, University of Applied Sciences and Arts of Southern Switzerland, Galleria 2, Via Cantonale 2c, CH-6928 Manno, Switzerland.

[8]Department Applied Science and Techology, Politecnico di Torino, Corso Duca degli Abruzzi 24, 10129 Torino, Italy.

E-mail: yagai@faculty.chiba-u.jp; Fax: +81-(0)43-290-3401; Tel: +81-(0)43-290-3169

**Mechanical interlocking of molecules (catenation) is a nontrivial challenge in modern synthetic chemistry and materials science[1,2]. One strategy to achieve catenation is the design of pre-annular molecules that are capable of both efficient cyclization and of pre-organizing another precursor to engage in subsequent interlocking[3–9]. This task is particularly difficult when the annular target is composed of a large ensemble of molecules, i.e., when the target is a supramolecular assembly. However, the construction of such unprecedented assemblies would enable the visualization of nontrivial nanotopologies through microscopy techniques, which would not only satisfy academic curiosity, but also pave the way to materials with nanotopology-derived properties. Herein, we report the synthesis of such a type of nanotopology using fibrous supramolecular assemblies with intrinsic curvature. Using a solvent-mixing strategy, we kinetically organized a molecule that can elongate into toroids with a radius of ca. 13 nm. Atomic force microscopy (AFM) on the resulting nanoscale toroids revealed a high percentage of oligo-catenation, which is sufficient to yield ‹ nanolympiadane› [10]. Spectroscopic and theoretical studies suggested that this unusually high degree of catenation stems from the secondary nucleation of the precursor molecules around the toroids. By modifying the self-assembly protocol to promote ring-closure and secondary nucleation, a maximum catenation number of 22 was confirmed by AFM.**

A crucial requirement for the bottom-up creation of an interlocked nanotopology is a molecular assembly system that can reproducibly provide annular nanostructures with a uniform diameter and sufficient inner void space. The topological supramolecular polymers that our group has explored over the past few years ideally satisfy this principal requirement[11]. We have developed a variety of barbiturated π-conjugated molecules that can form six-membered supermacrocycles, which we have termed ‹ rosettes› , through hydrogen bonds (Fig. 1a). The formation of these rosettes is coupled to the nucleation of supramolecular polymerization via π–π stacking of the rosettes with translational and

rotational displacement (Fig. 1b)[12,13]. The repetition of this specific rosette stacking induces a uniform, intrinsic curvature (radius: 7–13 nm; Fig. 1a), which eventually leads to the formation of supramolecular polymers with unprecedented topologies, including toroids[12–14], helicoids[15,16], and random coils (Fig. 1c)[16]. The topology of the polymers depends on the kinetics of the supramolecular polymerization, which can be controlled via the preparation protocol.

Based on the following observations, we chose **1** (Fig. 1a) as the monomer to realize unprecedented nanotopologies. Under thermodynamic control, e.g., slow cooling (~1.0 K min$^{-1}$) of a hot methylcyclohexane (MCH) solution of **1**, molecules of **1** organizes into helicoidal fibers through temperature-regulated supramolecular polymerization[16]. As increasing the cooling rate to 10 K min$^{-1}$, the topologies of the resulting polymers gradually change to randomly coiled structures. Upon abrupt cooling, i.e., thermal "quenching"[17], we obtained a small amount of toroids as kinetically trapped species that were formed via a ring-closing pathway (Supplementary Fig. 1). Ring-closure of the supramolecular polymers is further facilitated by promoting kinetic control of the polymerization via mixing different types of solvents. In this protocol, monomers concentrated in a good (polar) solvent (100 μL) were injected vigorously into 900 μL of a poor (less polar) solvent (Fig. 2a, Supplementary Video 1). As the monomer solution diffuses, the environment surrounding the monomers becomes less polar, initiating supramolecular polymerization. When chloroform and MCH were used as good and poor solvent, respectively, an atomic force microscopy (AFM) analysis (Supplementary Method and Supplementary Fig. 2) revealed that 44% of the monomers (total monomer concentration, $c_T = 1 \times 10^{-4}$ M) were kinetically trapped in toroid form (Fig. 2b,c and Supplementary Fig. 3a). It is noteworthy that 3% of the total toroids were obtained as geometrically interlocked nano-[2]catenanes under these conditions (Fig. 2b–d and Supplementary Fig. 3b).

The result that 3% of the toroids were obtained as nano-[2]catenanes motivated us to study another requirement for interlocked nanotopologies: templated supramolecular polymerization. Since simply

3

increasing the monomer concentration did not improve the nanocatenane yield (Supplementary Fig. 4), the formation of the nanocatenanes cannot be explained by the stochastic interlocking of growing toroids. Historically, the poor yield (<1%) obtained by stochastic catenation[8] during cyclization reactions was improved by covalent template strategies, but at the cost of a much longer synthetic route[18]. Sauvage and coworkers first overcame all the previous limitations and revolutionized the synthesis of catenanes by discovering template directed synthetic strategy, wherein annular and pro-annular components were preorganized using metal-ligand interactions[7]. The scope of this so-called template-directed approach has been expanded by other researchers using π-donor–acceptor interactions[6], hydrogen bonding[5], and the hydrophobic effect[3,4]. In our supramolecular polymers, which are covered with linear alkyl chains, preorganization of monomers via van der Waals interactions could potentially occur at the surface of the preformed toroids to facilitate heterogeneous nucleation (secondary nucleation; Fig. 1d)[19]. If this type of templated nucleation were to occur at the interior surface of the toroids, subsequent elongation and ring-closure of the resulting polymers would result in nano-[2]catenanes. On the other hand, if the secondarily nucleated fibers fail to close into toroids, the elongation of the open-ended fibers would lead to pseudorotaxanes (Fig. 2e and Supplementary Discussion 1).

Using a seeding experiment with separately prepared toroids[20–22], we assessed whether the secondary nucleation could occur in a solution of **1**. For this purpose, we initially established a method to isolate toroids from a complex mixture of supramolecular polymers with various topologies by exploiting their kinetic stability due to their lack of termini and relatively small size[23]. In brief, the open-ended short coils in a mixture of supramolecular polymers were selectively reorganized into elongated helical fibers with lengths >1 μm by thermal annealing (Fig. 2f and Extended Data Fig. 1a). The resulting elongated fibers could be readily filtered out from the toroids using a membrane filter with a pore size of 200 nm (Fig. 2f and Extended Data Fig. 1b). The toroid structure in solution was characterized by small-angle

X-ray and neutron scattering (SAXS, SANS) measurements, whose results showed good agreement with the results of AFM measurements and those of a model based on rosettes (Fig. 2i,j, Supplementary Figs. 5–7 and Supplementary Table 1)[12,24]. The toroid dimensions obtained by fitting analysis (toroid radius, $R = 12.5$ nm; cross-sectional radius excluding alkyl shell, $a = 2.5$ nm; aspect ratio, $b = 0.56$; alkyl shell width, $\delta = 1.6$ nm; number of rosettes per toroid, $N_{agg} = 100$) suggest an internal circular void with radius = 8.4 nm, which would certainly be capable of accommodating two fibers to generate nano-[n > 2]catenanes. The comparison of the SAXS and SANS data, which highlight different parts of the structure[12], and associated analysis clearly point to the fibers having a core-shell structure, in line with being formed by stacking of the rosettes, with the alkyl region outside a more electron-dense core. These alkyl regions are highly penetrated by solvent molecules (71% based on the SANS/SAXS analysis). Given the potential for alkyl chain overlap, it is therefore conceivable that the nano-[n ≥ 2]catenanes form by secondary nucleation of rosettes or monomers of **1** in these diffuse shells (Supplementary Discussion 2).

The isolated toroids are kinetically stable upon dilution to $c_T = 1 \times 10^{-6}$ M at 353 K, which is a prerequisite for their use as seeds. We thus added a small portion of the toroid solution to a large volume of monomer solution of **1** in MCH ($c_T = 5 \times 10^{-6}$ M) at 353 K and subsequently lowered the solution temperature to just below the elongation temperature ($T_e = 338$ K, Fig. 2g). As shown in Fig. 2h and Supplementary Fig. 8, the presence of toroids clearly accelerated the growth of an absorption band at 470 nm, associated with the π–π stacking of the diphenylnaphthalene cores[16]. As the elongation of the toroid seeds is topologically not possible due to lack of termini[20–22], the above observation clearly demonstrates that the toroids promote the secondary nucleation of monomers of **1** on their surface.

We further evaluated the reaction order associated with the secondary nucleation process of monomers by analyzing a set of aggregation kinetics data acquired for different concentrations of **1** in the absence

of seeds (Fig. 2k). In protein aggregation, the time required to consume half of the total amount of

monomers is referred to as the ⸴ half-time⸴ ($t_{50}$), and $t_{50}$ is related to the initial monomer concentration

($C_0$) via the scaling law

$$t_{50} \propto (C_0)^\gamma$$

where $\gamma$ is the scaling exponent[19]. In systems dominated by secondary nucleation processes, $\gamma$ is related

to the reaction order ($n_2$) according to:

$$\gamma = -(1 + n_2)/2$$

We thus plotted $\log(t_{50})$ as a function of $\log C_0$ in order to evaluate $\gamma$ (Fig. 2m)[19]. From the slope, we

found that $\gamma$ was equal to $-1.7$, which corresponds to an $n_2$ value of 2.4. This value is consistent with

monomer-dependent secondary processes, such as those observed in the kinetics of amyloid growth[19,25],

suggesting that significant secondary nucleation occurs in the present system.


We used multiscale molecular simulations to study the event of a secondary nucleation occurring on the

surface of pre-existing toroids (or oligomers) in MCH. To deal with the complex hierarchical nature of

the system, we developed coarse-grained (CG) models for the rosettes (Fig. 3a) reliably capturing their

structural behavior and the rosette–rosette interactions in solution, while at the same time allowing us to

study their assembly on a sufficiently large scale (see Supplementary Computational Details). The

results of these simulations indicate that solvophobic interactions can make the self-assembly of rosettes

more likely to initiate on the surface of preformed toroids. CG molecular dynamics simulations showed

a strong propensity of the rosettes to axial stacking. However, it was also observed that these may

interact with the surface of oligomers formed in the system, which is consistent with the experimentally

suggested secondary nucleation on the toroids. To obtain a tangible evidence of such a scenario, we

created a CG model of a toroid composed of prestacked rosettes having size consistent with the

experimental one (blue part in Fig. 3a). A portion of this toroid (blue part in Fig. 3a) was used in

metadynamics simulations[26] allowing to study the interaction of one single rosette or of a rosette trimer

(Fig. 3b, in red) with the toroid surface[27]. In Fig. 3b, we plot the free-energy profile for the interaction between the rosette trimer and the toroid as a function of the distance ($d$) between their centers (the same simulation with a single rosette provided analogous results). This shows strong affinity, suggesting that preassembled rosette toroids work as nucleation seeds for the growth of other ones onto their surface in MCH. The formation of catenanes would then be related to the statistical probability for the toroids to close-up in such a way to form mechanically interlocked topologies (Fig. 1d).

Given that the solute–solute interactions that play a critical role in secondary nucleation are affected by the solvent[28], we also evaluated the reaction order in $n$-octane as a representative $n$-alkane solvent (Fig. 2l). The corresponding $\gamma$ ($-2.9$) and $n_2$ (4.8) values suggest a higher tendency toward secondary nucleation in $n$-octane (Fig. 2m). In line with this finding, much higher proportions of toroids were catenated when we used $n$-alkanes ($n$-hexane to $n$-decane) as the poor solvent (Fig. 3c, Extended Data Fig. 2 and Supplementary Figs. 3b and 9). It should be noted that the overall toroid yield decreased in linear alkane solvents compared to cyclic alkanes (MCH and cyclohexane) because the open-elongation pathway becomes more feasible with decreasing solvent polarity (Fig. 3c and Supplementary Figs. 3a and 10). The use of longer $n$-alkanes ($n$-undecane and $n$-dodecane) was not effective due to agglomeration of assemblies (Supplementary Fig. 11). Surprisingly, we found even longer congeners (Fig. 3d–f and Extended Data Fig. 3a) such as nano-[5]catenane in $n$-octane, which we coined 'nanolympiadane' (length: ~80 nm; Extended Data Fig. 3b,c) in homage to the [5]catenane system first reported by Stoddart and colleagues[10]. Its topology, visualized by AFM, is impressively similar to the Olympic rings, although in our nanolympiadane, the five rings do not adopt the helical orientation seen in the Olympic logo (Fig. 3g and Extended Data Fig. 4), which is most likely due to the adsorption of the structure on the highly oriented pyrolytic graphite (HOPG) substrate surface.

In order to prepare further elongated nanocatenanes, the mechanism for the spontaneous self-assembly of the aforementioned oligomeric nanocatenanes should be considered. Rowan *et al.* have recently reported the synthesis of poly[n]catenanes with [4 ≤ n ≤ 130] by interlocking 68-membered macrocyclic ditopic ligands and a cyclizable threading molecule[9]. The metallo-supramolecular polymer templates, whose degree of polymerization practically determines the degree of polycatenation, were preassembled by the addition of $Zn^{2+}$. In the present system, preassembly of such templates is obviously impossible, and elongation of the catenanes must occur in a stepwise manner (Fig. 4a). Accordingly, increasing local concentrations by injecting all the monomer at once would not be effective to increase [n]. Instead, a portion-wise injection protocol would more likely provide conditions in which monomers could be fed to preformed toroid seeds upon each injection in a living manner[19,20]. Furthermore, the portion-wise injection of monomer would probably result in lower local monomer concentration, which would facilitate secondary nucleation[28–30] as well as reduce the occurrence of the unwanted open-elongation pathway leading to randomly coiled fibers.

We thus injected the monomer solution in ten portions (one 10 µL injection per second; Fig. 4b, Supplementary Video 2). As shown in Fig. 4c, Extended Data Fig. 5 and Supplementary Fig. 12, this approach increased both the overall toroid yield and the proportion of catenanes using *n*-alkane as well as cycloalkane solvents. For example, ten-injections into *n*-octane provided a toroid yield of 49% based on the monomer (Extended Data Fig. 5 and Supplementary Fig. 12), 41% of which were catenated (Fig. 4c). The catenation number [n] was even more strongly affected than the overall catenane yield. Although ⟨ n ⟩ rarely exceeded 5 in single-injection experiments using *n*-alkanes, the ten-injections method produced nano-poly[n]catenanes whose ⟨ n ⟩ values beyond 7 (Fig. 4d–g and Extended Data Fig. 6). Fig. 4e–g show nano-poly[17], [18] and [22]catenanes. In these samples, the number of toroids that form nano-poly[n ≥ 3]catenanes is higher than that of nano-[2]catenanes (Fig. 4d). This result suggests that a cooperativity might be responsible for the polycatenation, presumably because two

interlocked toroids can provide a specific nanospace that facilitates secondary nucleation more effectively than the surface of single toroids. The elongated catenanes are stable in solution for months, suggesting that the toroidal constituents are kinetically stable against chain-breaking and interchain end-to-end connection as well as reorganization through monomer exchange.

We have demonstrated that the controlled use of secondary nucleation is an effective strategy to create mechanically interlocked nanostructures. Similar approaches could be applied to other macromolecular systems based on covalent or noncovalent polymerization. The purification of nanocatenanes is also an important challenge in order to investigate the physical properties of these topologically exotic molecular assemblies. We have already succeeded in separating toroid-based topologies (nano-[n]catenanes and single toroids) from open-ended species via the thermal reorganization of the open-ended short fibers into elongated helical fibers and subsequent membrane filtration. We envisage that further catenation (n > 100) by enhancing the aforementioned cooperativity would allow us to purify those elongated species, which could lead to the discovery of unprecedented physical properties arising from mesoscopic topologies.

**Competing interests**

The authors declare no competing interests.

**Data availability**

The authors declare that all other data supporting the findings of this study are available within the paper and its supplementary information files.

**Code availability**

There is no experiment requiring custom code or mathematical algorithm.

1.   Segawa, Y. et al. Topological molecular nanocarbons: all-benzene catenane and trefoil knot. *Science* **365**, 272–276 (2019).

2.  Leigh, D. A., Pritchard, R. G. & Stephens, A. J. A star of David catenane. *Nat. Chem.* **6**, 978–982 (2014).

3.  Li, H. et al. Quantitative self-assembly of a purely organic three-dimensional catenane in water. *Nat. Chem.* **7**, 1003–1008 (2015).

4.  Fujita, M., Ibukuro, F., Hagihara, H. & Ogura, K. Quantitative self-assembly of a [2]catenane from two preformed molecular rings. *Nature* **367**, 720–723 (1994).

5.  Hunter, C. A. Synthesis and structure elucidation of a new [2]-catenane. *J. Am. Chem. Soc.* **114**, 5303–5311 (1992).

6.  Ashton, P. R. et al. A [2]catenane made to order. *Angew. Chem. Int. Ed. Engl.* **28**, 1396–1399 (1989).

7.  Dietrich-Buchecker, C. O., Sauvage, J. P. & Kintzinger, J. P. Une nouvelle famille de molecules: les metallo-catenanes. *Tetrahedron Lett.* **24**, 5095–5098 (1983).

8.  Wasserman, E. Chemical topology. *Sci. Am.* **207**, 94–102 (1962).

9.  Wu, Q. et al. Poly[*n*]catenanes: synthesis of molecular interlocked chains. *Science* **358**, 1434–1439 (2017).

10. Amabilino, D. B., Ashton, P. R., Reder, A. S., Spencer, N. & Stoddart, J. F. Olympiadane. *Angew. Chem. Int. Ed. Engl.* **33**, 1286–1290 (1994).

11. Yagai, S., Kitamoto, Y., Datta, S. & Adhikari, B. Supramolecular polymers capable of controlling their topology. *Acc. Chem. Res.* **52**, 1325–1335 (2019).

12. Hollamby, M. J. et al. Simultaneous SAXS and SANS analysis for the detection of toroidal supramolecular polymers composed of noncovalent supermacrocycles in solution. *Angew. Chem. Int. Ed.* **55**, 9890–9893 (2016).

13. Yagai, S. et al. Self-organization of hydrogen-bonding naphthalene chromophores into J-type nanorings and H-type nanorods: impact of regioisomerism. *Angew. Chem. Int. Ed.* **51**, 6643–6647 (2012).

14. Adhikari, B., Aratsu, K., Davis, J. & Yagai, S. Photoresponsive circular supramolecular polymers: a topological trap and photoinduced ring-opening elongation. *Angew. Chem. Int. Ed.* **58**, 3764–3768 (2019).

15. Adhikari, B. et al. Light-induced unfolding and refolding of supramolecular polymer nanofibres. *Nat. Commun.* **8**, 15254 (2017).

16. Prabhu, D. D. et al. Self-folding of supramolecular polymers into bioinspired topology. *Sci. Adv.* **4**, eaat8466 (2018).

17. Korevaar, P. A. et al. Pathway complexity in supramolecular polymerization. *Nature* **481**, 492–496 (2012).

18. Gil-Ramírez, G., Leigh, D. A. & Stephens, A. J. Catenanes: fifty years of molecular links. *Angew. Chem. Int. Ed.* **54**, 6110–6150 (2015).

19. Cohen, S. I. A., Vendruscolo, M., Dobson, C. M. & Knowles, T. P. J. From macroscopic measurements to microscopic mechanisms of protein aggregation. *J. Mol. Biol.* **421**, 160–171 (2012).

20. Ogi, S., Sugiyasu, K., Manna, S., Samitsu, S. & Takeuchi, M. Living supramolecular polymerization realized through a biomimetic approach. *Nat. Chem.* **6**, 188–195 (2014).

21. Wang, X. et al. Cylindrical block copolymer micelles and co-micelles of controlled length and architecture. *Science* **317**, 644–647 (2007).

22. Zhang, W. et al. Supramolecular linear heterojunction composed of graphite-like semiconducting nanotubular segments. *Science* **334**, 340–343 (2011).

23. Suzuki, A. et al. Topological impact on the kinetic stability of supramolecular polymers. *J. Am. Chem. Soc.* **141**, 13196–13202 (2019).

24. Breßler, I., Kohlbrecher, J. & Thünemann, A. F. *SASfit*: a tool for small-angle scattering data analysis using a library of analytical expressions. *J. Appl. Cryst.* **48**, 1587–1598 (2015).

25. Meisl, G. et al. Molecular mechanisms of protein aggregation from global fitting of kinetic models. *Nat. Protoc.* **11**, 252–272 (2016).

26. Laio, A. & Parrinello, M. Escaping free-energy minima. *Proc. Natl Acad. Sci. USA* **99**, 12562–12566 (2002).

27. Bochicchio, D., Salvalaglio, M. & Pavan, G. M. Into the dynamics of a supramolecular polymer at submolecular resolution. *Nat. Commun.* **8**, 147 (2017).

28. Anwar, J., Khan, S. & Lindfors, L. Secondary crystal nucleation: nuclei breeding factory uncovered. *Angew. Chem. Int. Ed.* **54**, 14681–14684 (2015).

29. Kondepudi, D. K. & Asakura, K. Chiral autocatalysis, spontaneous symmetry breaking, and stochastic behavior. *Acc. Chem. Res.* **34**, 946–954 (2001).

30. Kondepudi, D. K., Kaufman, R. J. & Singh, N. Chiral symmetry breaking in sodium chlorate crystallizaton. *Science* **250**, 975–976 (1990).
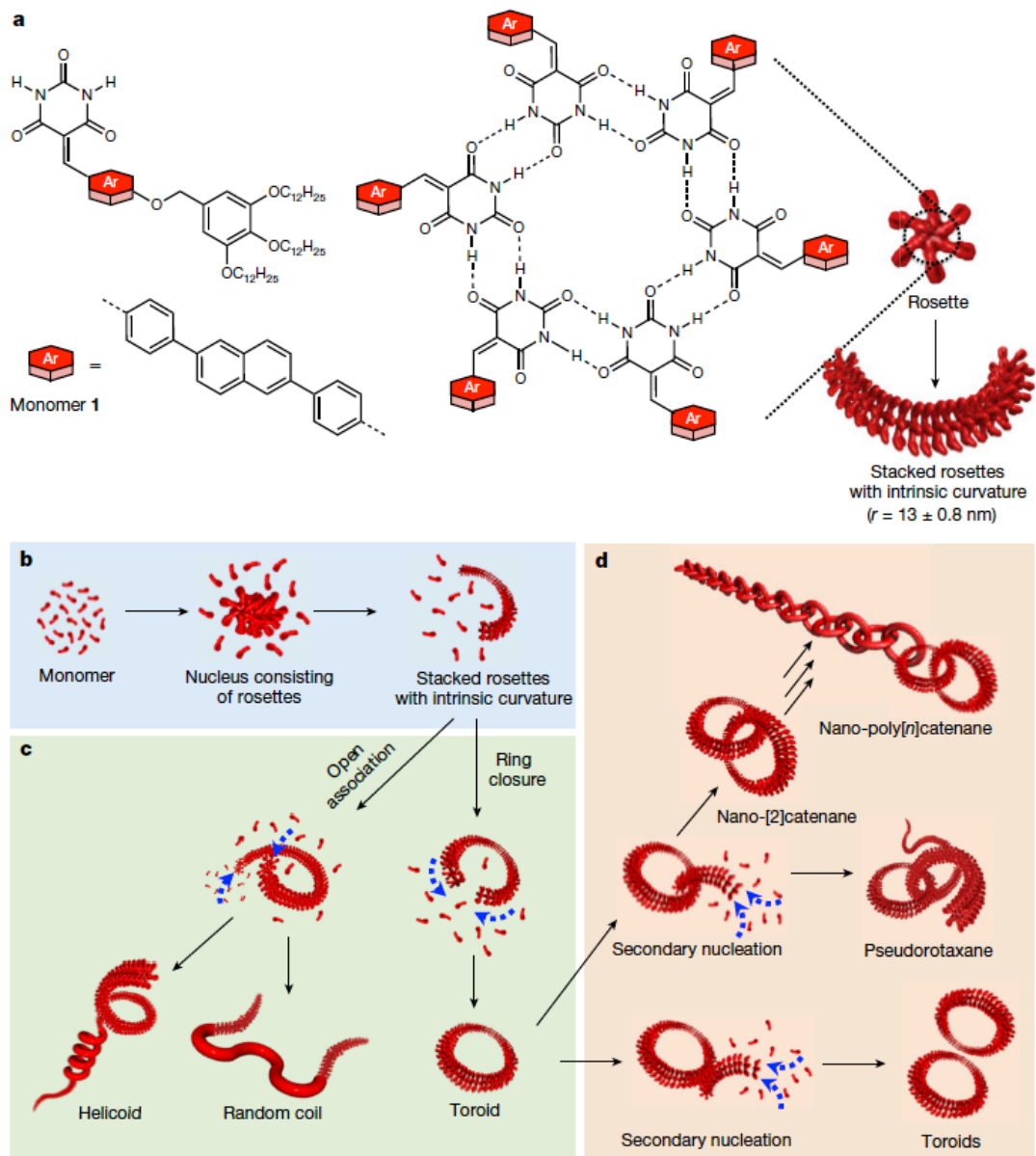
**Figure 1 | Self-assembly of a barbiturated monomer into various supramolecular polymer topologies. a**, Chemical structure of barbiturated naphthalene derivative **1** and a schematic representation of the unique stacking of its hydrogen-bonded cyclic hexamers (rosettes) to generate an intrinsic curvature. **b**, **c**, Schematic illustration of the primary nucleation (**b**) and elongation (**c**) of the monomers into distinct nanotopologies. **d**, Schematic illustration of secondary nucleation on a toroid to produce mechanically interlocked topologies.
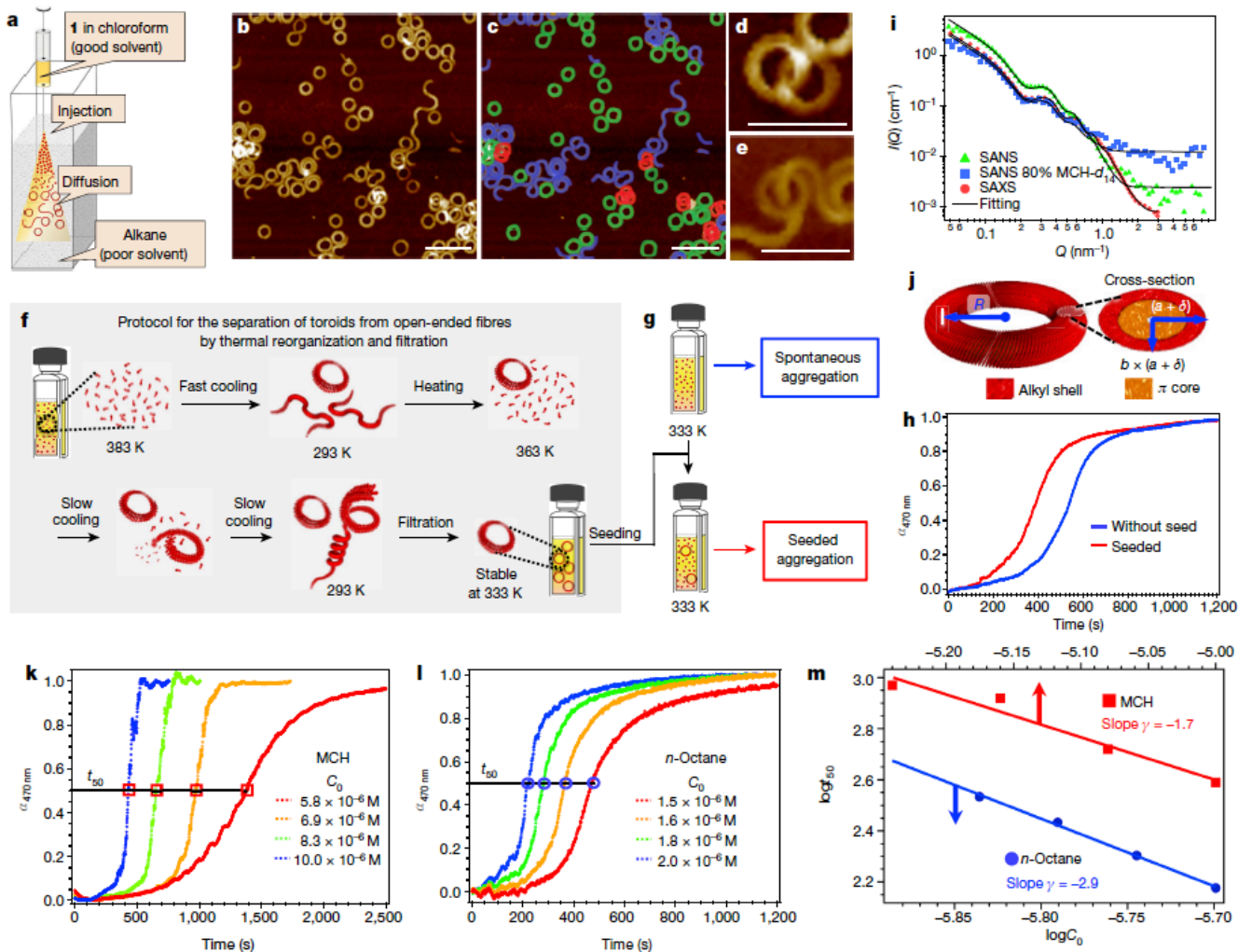
**Figure 2 | Supramolecular polymerization protocols. a**, Depiction of the solvent-mixing protocol. **b–e**, AFM image of supramolecular polymers obtained by injecting a 100 μL chloroform solution of **1** ($c_T$ = 1 × 10⁻³ M) into 900 μL of MCH in one portion; scale bars = 100 (**b** and **c**) and 50 (**d** and **e**) nm. **c**, a complex mixture; **d**, nano-[2]catenane; **e**, pseudorotaxane. Image **c** is a duplicate of image **b**, but different topologies are colored to estimate the relative area: blue, green and red for open-ended coils, single toroids and mechanically interlocked toroids, respectively. **f**, **g**, Protocols for separating toroids from open-ended fibers (**f**) and seeded supramolecular polymerization (**g**). **h**, Comparison of the time-dependent changes in the molar fractions of aggregates of **1** ($\alpha_{470 \text{ nm}}$, monitored at wavelength $\lambda$ = 470 nm) in a monomeric MCH solution ($c_T$ = 4.8 × 10⁻⁶ M) at 333 K in the presence (red dots) and absence (blue dots) of toroid seeds ([seed] = 1.6 × 10⁻⁶ M based on the monomers). **i**, SANS (green triangles and blue squares) and SAXS (red circles) data of **1** ($c_T$ = 5 × 10⁻⁴ M) in MCH-$d_{14}$ (green triangles) and a mixed solvent comprising 80% MCH-$d_{14}$ and 20% MCH-$h_{14}$ (blue squares). Black solid lines represent fits of the data, using a toroid form factor and a flat background. **j**, Representation of the core (orange)-shell (red) toroid of **1** with parameters obtained from model fitting of the SAS data ($R$, $a$, $\delta_{\text{shell}}$, $b$). **k**, **l**, Time-dependent changes of $\alpha_{470 \text{ nm}}$ of **1** at various $C_0$ in MCH (**k**) and $n$-octane (**l**) at 333 K in the absence of toroid seeds. **m**, Log–log plot of the time required for $C_0$ to drop by 50% in the seeded experiments in MCH (red squares) and $n$-octane (blue circles) as a function of $C_0$.

15
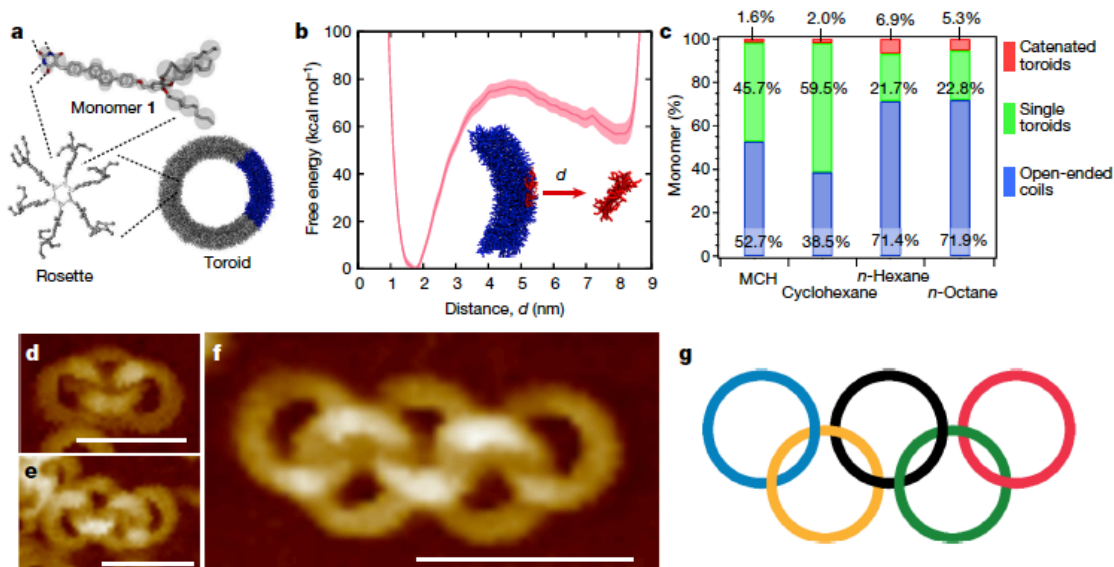
**Figure 3 | Solvent dependence of the catenane yield. a**, All atom (AA) and coarse-grained (CG) models of one monomer, one rosette (hexagonal assembly of six monomers) and one toroid of **1** used in the simulations. **b**, Free-energy profile for the interaction between one rosette trimer and the surface of the toroid (a portion of a full toroid composed of 50 rosettes) as a function of the distance ($d$) between the center of the toroid section (blue) and the center of the rosette trimer (red). **c**, Histogram showing the yield of catenanes (red bar), toroids (green bar), and random coils (blue bar) depending on the choice of poor solvent in single-injection solvent mixing experiment. **d**–**f**, AFM images of nano-[3]catenane (**d**), nano-[4]catenane (**e**), and nano-[5]catenane (**f**) obtained by injecting 100 μL of a chloroform solution of **1** ($1 \times 10^{-3}$ M) into 900 μL of *n*-octane in one portion; scale bars = 50 nm. **g**, Symbol of the Olympic rings; reproduced with permission from the International Olympic Committee.
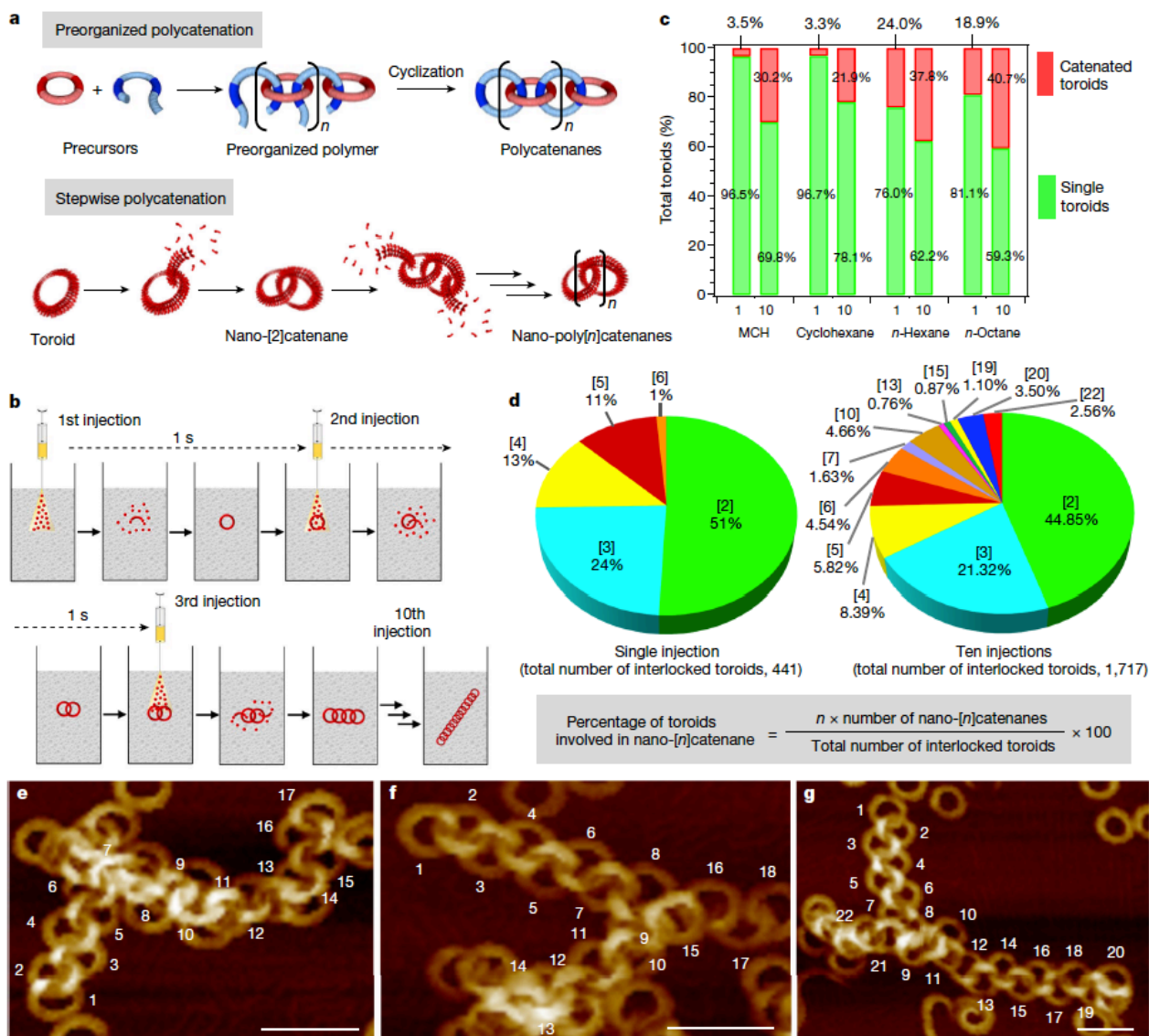
**Figure 4 | Nano-polycatenanes. a**, Schematic illustration of polycatenation by preorganization and stepwise manner. **b**, Depiction of a ten-injections solvent-mixing experiment. **c**, Histogram comparing the yields of interlocked toroids (red bar) and single toroids (green bar) with respect to the overall toroids for different poor solvents and number of monomer solution injections. **d**, Pie charts showing the percent interlocked toroids constituting various nano-[n]catenanes for one hundred $500 \times 500$ nm$^2$ AFM images acquired after the single-injection (left) and ten-injections (right) solvent-mixing experiments with chloroform and *n*-octane as the good and poor solvent, respectively ($c_T = 1 \times 10^{-4}$ M after solvent mixing). **e–g**, AFM images of nano-poly[17]catenane (**e**), nano-poly[18]catenane (**f**), and nano-poly[22]catenane (**g**) obtained by injecting ten portions (one per second) of 10 μL of a chloroform solution of **1** ($1 \times 10^{-3}$ M) into 900 μL of poor solvent. Nano-poly[17]catenane (**e**) was obtained when *n*-hexane was used as the poor solvent; nano-poly[18]catenanes (**f**) and nano-poly[22]catenanes (**g**) were obtained using *n*-octane as the poor solvent; inset numbering shows counting of interlocked toroids of nano-poly[n]catenanes; scale bars = 50 nm. For these catenanes, branched catenation likely occurred at for example, toroid #7 and #13 in **e**, #9 in **f**, and #8 in **g** via threading of a supramolecular polymer fiber through an already-catenated toroid, which would seem to be sterically challenging unless the fibers grow in an organized fashion from secondary nuclei generated at the inner surface of the preformed catenanes.

17

**Methods**

**Single-injection and ten-injections solvent mixing experiments**

A stock monomer solution ($c_T = 1 \times 10^{-3}$ M) was prepared by dissolving 1.08 mg of compound **1** in 1 mL chloroform (good solvent). In a typical single-injection solvent mixing experiment, 100 μL of the chloroform solution taken in a Hamilton syringe (volume = 100 μL) was injected in one portion into 900 μL of MCH (poor solvent) taken in a glass vial at 293 K (Supplementary Video 1). On the other hand, a typical ten-injections solvent mixing experiment was performed by injecting the same volume of the monomer solution of **1** ($c_T = 1 \times 10^{-3}$ M) in ten portions (one 10 μL injection per approximately second) into 900 μL of MCH taken in a glass vial at 293 K (Supplementary Video 2). The final concentration of **1** in the solution obtained after solvent mixing is $1 \times 10^{-4}$ M for both experiments.

**Preparation of toroid seeds and seeding experiment**

A hot (383 K) solution (1 mL, $1 \times 10^{-4}$ M) of **1** in MCH/CHCl₃ (9:1, v/v) was quenched into an ice bath for 30 s to obtain a mixture of toroids and randomly coiled small fibers. The quenched solution was heated at 363 K for 5 min to dissociate the small fibers into monomers selectively, while the toroids remained intact by the virtue of their superior kinetic stability[23]. 9:1 is the best ratio for mixing MCH and CHCl₃ to get nearly pure toroid solutions. Upon subsequent cooling the solution to 293 K at a cooling rate of 1 K min⁻¹, the monomers were polymerized into elongated helical fibers with length exceeding 1 μm. The resulting solution was passed through a membrane filter with pore size of 200 nm to remove the helical fibers, while the toroids remained predominantly in the filtrate. From the absorbance of the filtrate, the concentration of **1** that formed toroids was estimated to be $5 \times 10^{-5}$ M. The solvent was carefully evaporated using a flow of N₂ to get a film of toroids which was then dispersed in 1 mL MCH by mechanical shaking. The solvent evaporation followed by dispersion in MCH did not affect the structural integrity of the toroids as confirmed by AFM.

In a typical seeding experiment, 100 μL of the MCH solution ($5 \times 10^{-5}$ M) containing toroid seeds was added to a monomer solution (3 mL, $5 \times 10^{-6}$ M, $T_e = 338$ K) in MCH at 353 K. The final concentrations of monomer and seed are $4.8 \times 10^{-6}$ and $1.6 \times 10^{-6}$ M, respectively. Then, the kinetics of the seeded supramolecular polymerization of **1** was studied at 333 K by UV–Vis spectroscopy to follow the growth of a new absorption band at $\lambda = 470$ nm, which is attributed to π–π stacking of the diphenylnaphthalene core[16]. In the seeded experiment, the residual absorption of the toroid seeds was automatically subtracted from the solution containing the mixture of seed and monomers by using a double-beam UV-Vis spectrophotometer.

**Analysis of seeded supramolecular polymerization**

Time-dependent changes in the molar fractions of aggregates of **1**, $\alpha_{(470\ nm)}$, at a certain temperature ($T$) in the presence and absence of toroid seeds was calculated from the absorption intensity at $\lambda = 470$ nm based on the following equation:

$$\alpha_{470} = [\text{Abs}_{470}(T) - \text{Abs}_{470}(fully\ monomeric)] / [\text{Abs}_{470}(fully\ aggregated) - \text{Abs}_{470}(fully\ monomeric)]$$

where $\text{Abs}_{470}(T)$ is the absorption intensity at a given temperature ($T$), $\text{Abs}_{470}(fully\ monomeric)$ and $\text{Abs}_{470}(fully\ aggregated)$ are the absorbance of the purely monomeric state (at the highest temperature) and fully aggregated state (at the lowest temperature), respectively. The UV-Vis spectra used for the seeding experiment are shown in Supplementary Figure 13.
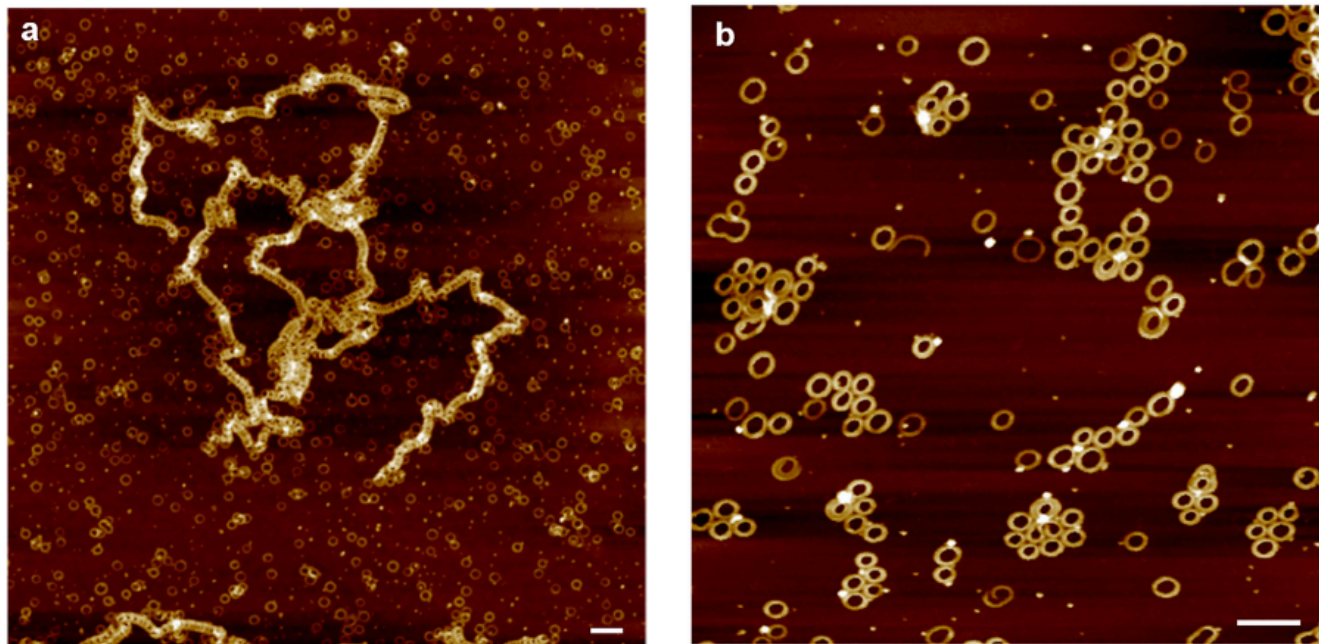
**Extended Data Fig. 1 | Separation of toroids from elongated fibers via thermal reorganization followed by membrane filtration. a**, AFM image of supramolecular polymers obtained by heating a quenched solution of **1** ($c_T = 1 \times 10^{-4}$ M) in MCH/CHCl$_3$ (9:1, v/v) at 363 K for 5 min and subsequently cooling to 293 K at a cooling rate of 1.0 K min$^{-1}$. **b**, AFM image of supramolecular polymers obtained after passing the resulting solution through a membrane filter with pore size of 200 nm. The samples were spin-coated onto a HOPG substrate at 293 K; scale bars = 100 nm.
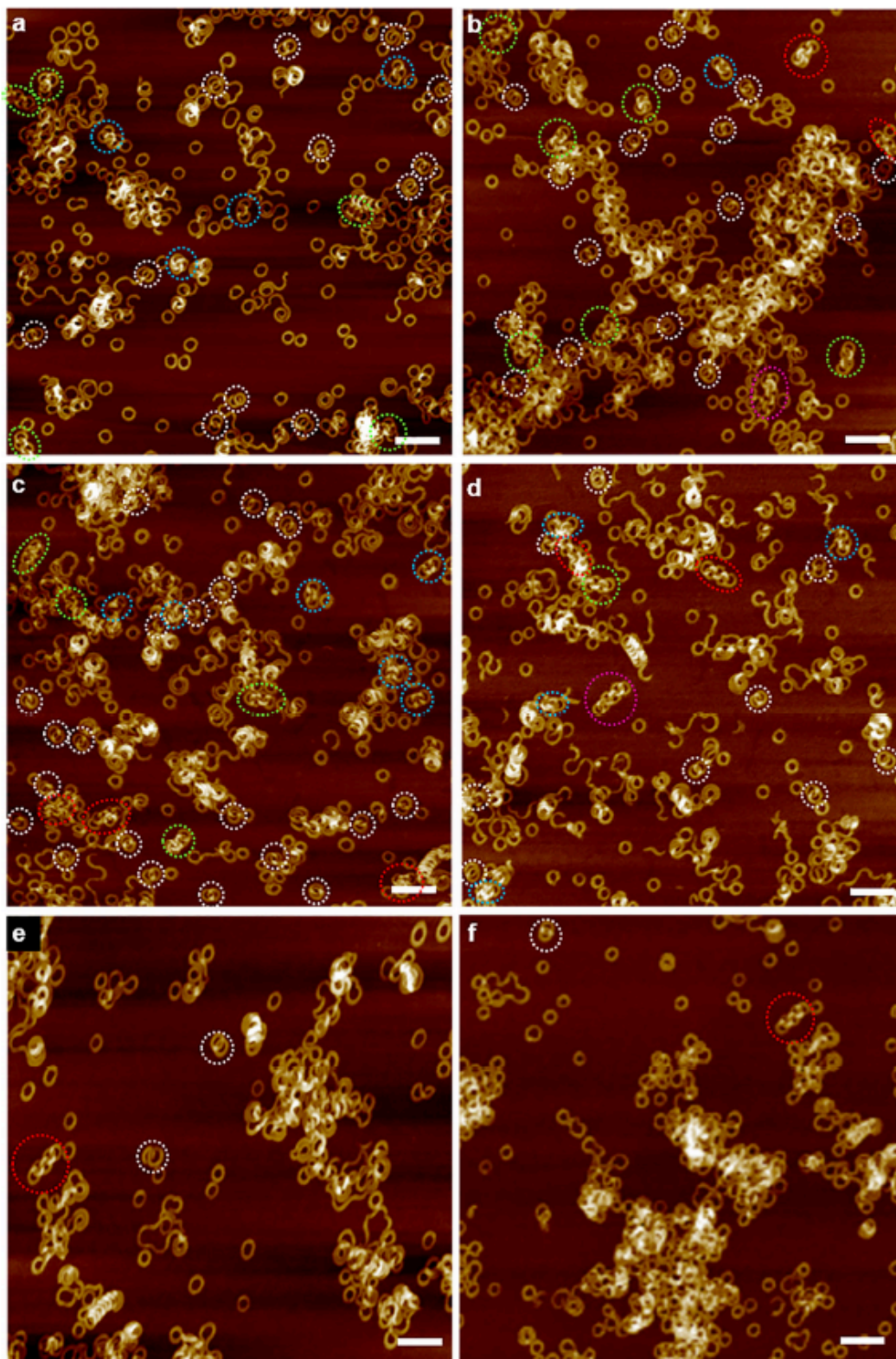
**Extended Data Fig. 2 | AFM images of supramolecular polymers obtained in various *n*-alkanes by single-injection solvent mixing experiment. a–f,** AFM images of supramolecular polymers prepared by injecting a 100 μL chloroform solution of **1** (1 × 10$^{-3}$ M) into 900 μL of *n*-hexane (**a**), *n*-heptane (**b**), *n*-octane (**c** and **d**), *n*-nonane (**e**), or *n*-decane (**f**) in one portion. Nano-[2], [3], [4], [5] and [6]catenanes are shown by dashed white, blue, green, red and pink circles, respectively. The samples were spin-coated onto a HOPG substrate at 293 K; scale bars = 100 nm.
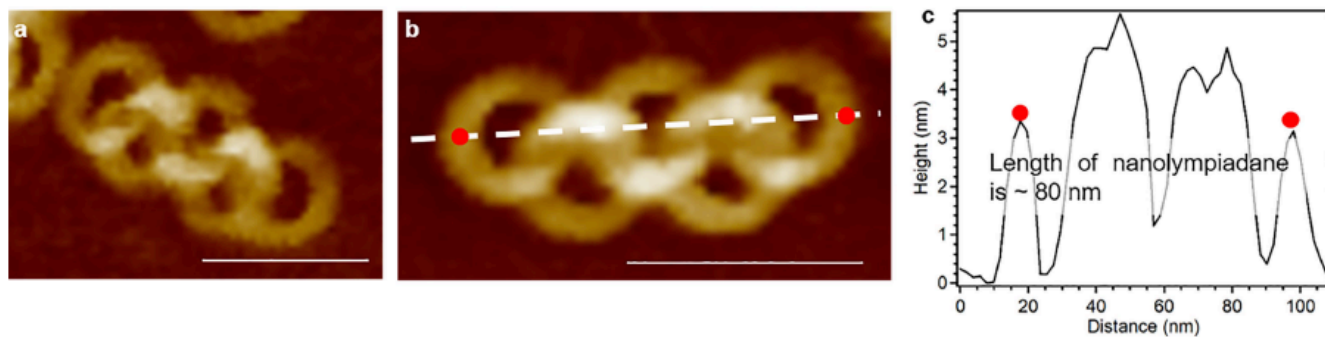
**Extended Data Fig. 3 | AFM images and height profile analysis of "nanolympiadane". a, b,** AFM images of "nanolympiadane" obtained by injecting 100 μL of a chloroform solution of **1** ($1 \times 10^{-3}$ M) into 900 μL of *n*-octane in one portion; **c,** AFM height profile analysis of a "nanolympiadane"; scale bars = 50 nm.
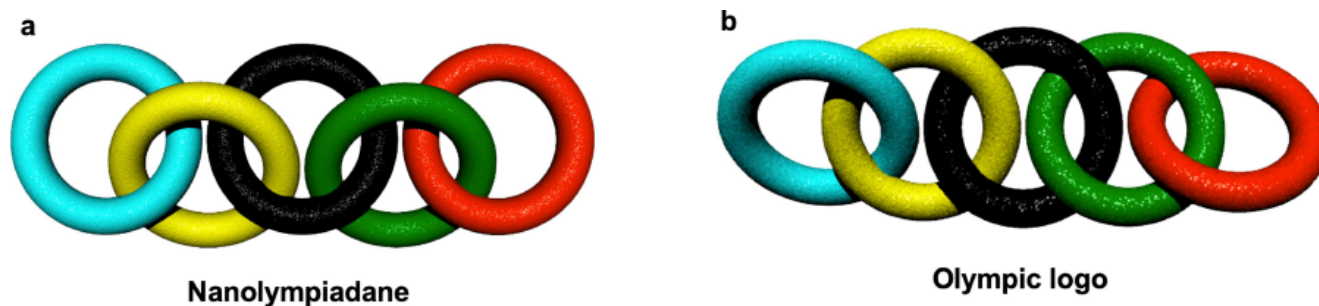


**Extended Data Fig. 4 | 3D representations of "nanolympiadane" and Olympic logo. a,** 3D arrangement of five toroids in our "nanolympiadane" on HOPG surface. **b,** 3D representation of five toroids deduced from the 2D representation of the Olympic logo.
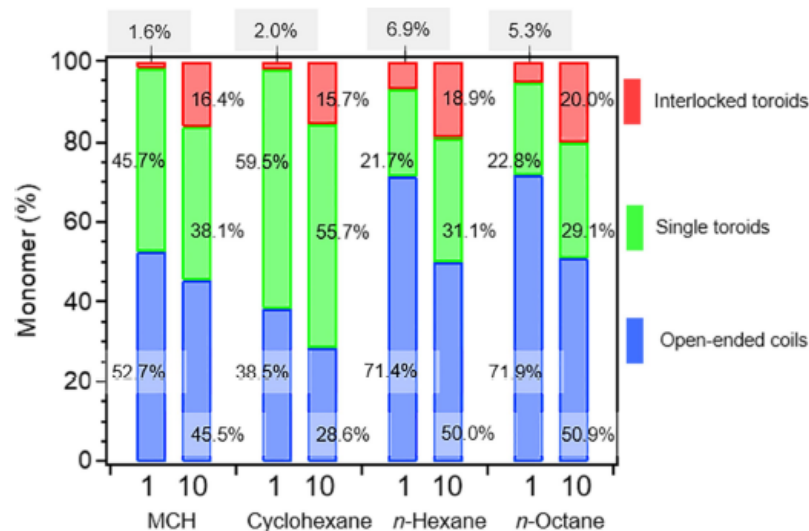
**Extended Data Fig. 5 | Yields of various supramolecular polymer topologies in different poor solvents depending on the number of monomer solution injections.** Histogram showing the yield of catenanes (red bar), toroids (green bar), and random coils (blue bar) depending on the choice of poor solvent and the number of injections of monomer solution.
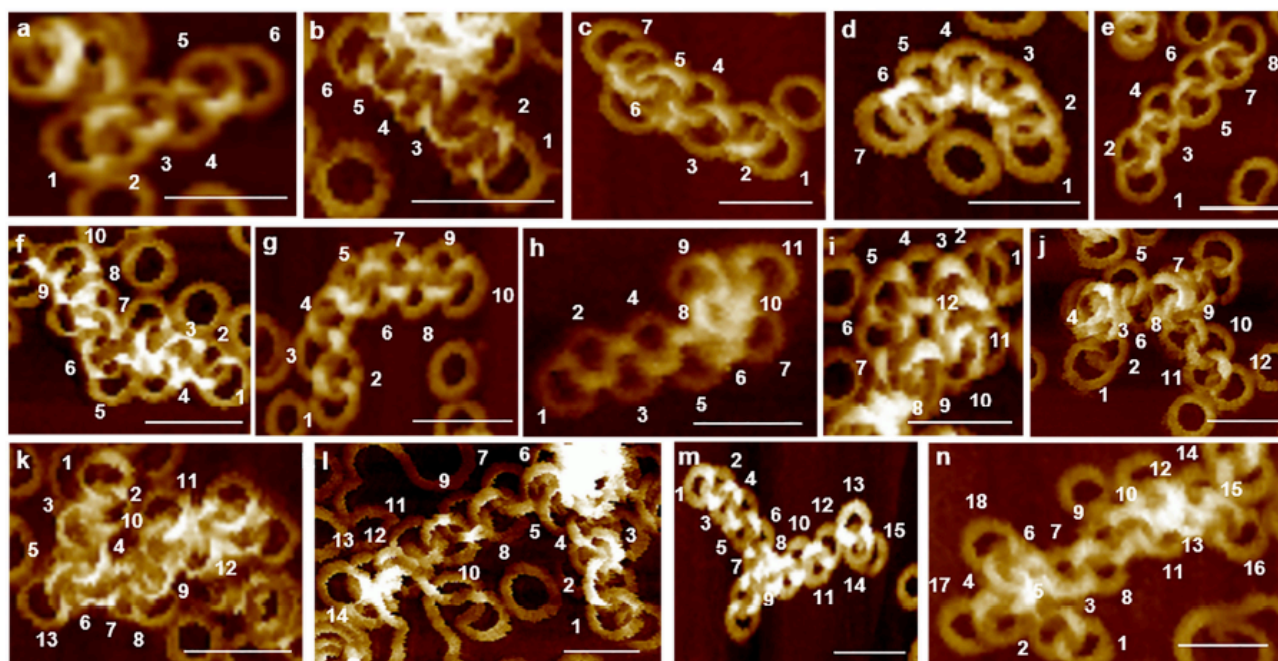


**Extended Data Fig. 6 | Additional AFM images of nano-poly[n]catenanes. a–n,** AFM images of nano-[6] (**a** and **b**), nano-poly[7] (**c** and **d**), [8] (**e**), [10] (**f** and **g**), [11] (**h**), [12] (**i** and **j**), [13] (**k**), [14] (**l**), [15] (**m**), and [18] (**n**) catenanes obtained by injecting ten portions (one per second) of 10 μL of a chloroform solution of **1** (1 × 10⁻³ M) into 900 μL of poor solvent; nano-[6] (**a** and **b**), nano-poly[7] (**c**), [8] (**e**), [11] (**h**), [12] (**j**), [13] (**k**), [14] (**l**), [15] (**m**), and [18] (**n**) catenanes were obtained using *n*-octane as poor solvent; nano-poly[7] (**d**), [10] (**f** and **g**), and [12] (**i**) catenanes were obtained when cyclohexane (**d** and **i**) and MCH (**f** and **g**) were used as poor solvents. The samples were spin-coated onto a HOPG substrate at 293 K; inset numbering shows counting of interlocked toroids of nano-[n]catenanes and nano-poly[n]catenanes; scale bars = 50 nm.